JOC Article

A FMO-Controlled Reaction Path in the Benzil−Benzilic Acid Rearrangement

Shinichi Yamabe,* Noriko Tsuchida, and Shoko Yamazaki

Department of Chemistry, Nara University of Education, Takabatake-cho, Nara 630-8528, Japan

yamabes@nara-edu.ac.jp

Received September 5, 2005

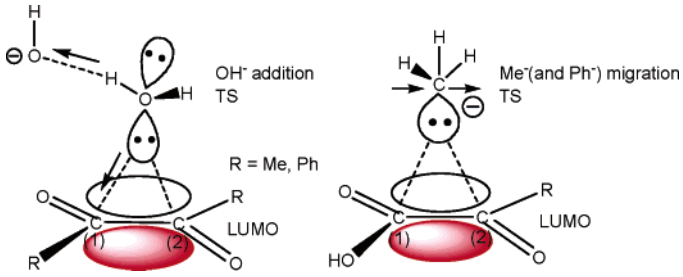

Reaction paths for the title rearrangement along with its methyl analogue were investigated by density functional theory calculations. The reaction model is R−CO−CO−R + $OH^-(H_2O)_4$ → $R_2C(OH)-COO^-$ + $(H_2O)_4$ (R = Me and Ph), where the water tetramer is employed both for solvation to OH^- and for the proton relay along hydrogen bonds. The reaction is composed of OH^- addition, C−C rotation, carbanion [1,2] migration, and proton relay toward the product anions. The rate-determining step was calculated to be the carbanion migration. Apparently, carbanion [1,2] migration is unlikely relative to the carbonium ion one. However, LUMOs of the 1,2-diketones have large and nodeless lobes at the reaction center, the C(1)−C(2) bond. The specific LUMO character is reflected both in the [2+1]-like one-center nucleophilic addition and in the carbanion [1,2] shift. The proton relay involved in the isomerization from the oxo intermediate to the carboxylate was calculated to take place via the water tetramer.

I. Introduction

Benzil, Ph−CO−CO−Ph (**1**), is a nonenolizable 1,2-diketone that undergoes a base-catalyzed rearrangement to yield the anion of an α-hydroxy acid, benzilate anion $Ph_2C(OH)CO_2^-$.[1] The reaction is believed to follow the pathway in Scheme 1. The rate-determining step is presumably the migration of the phenyl group in the initial OH^- adduct, i.e., **2** → **3**.[2] This is basically the analogue for 1,2-diketones of the intramolecular Cannizzaro reaction on the 1,2-dialdehyde glyoxal, OHC−CHO. In the former, it is the Ph^- anion that migrates to the adjacent C=O group. In the latter it was a hydride ion that migrates. Aliphatic 1,2-diketones also undergo the rearrangement, e.g., *tert*-butyl 2,3-dioxobutyrate and cyclohexane-1,2-dione.[3]

SCHEME 1

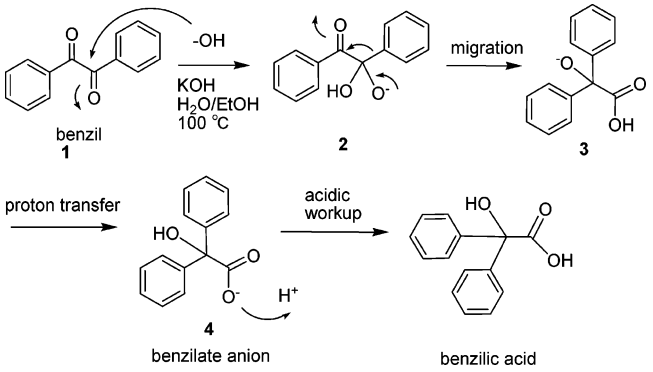

Although the benzilic acid rearrangement is a well-known foundamental organic reaction (consisting of only C, H, and O atoms) and a classic reaction (since 1838), its mechanism has not been studied in detail, and there have been no computational studies. While carbonium ion [1,2] shifts such as the pinacol and Wagner−Meerwein rearrangements are familiar,[4] carbanion

(1) (a) Liebig, J. *Justus Liebigs Ann. Chem.* **1838**, *25*, 27. (b) Zinin, N. *Justus Liebigs Ann. Chem.* **1839**, *31*, 329. (c) Selman, S.; Eastham, J. F. *Q. Rev. Chem. Soc.* **1960**, *14*, 221. (d) Gill, G. B. In *Comrehensive Organic Synthesis*; Trost, B. M., Fleming, I., Eds.; Pergamon Press: Elmosford, NY, 1991; Vol. 3, p 821.

(2) Sykes, P. *A Guidebook to Mechanism in Organic Chemistry*, 5th ed.; Longman Group Ltd.: London and New York, 1981; Chapter 8.4.10.

10.1021/jo051862r CCC: $33.50
Published on Web 02/03/2006

SCHEME 2. Orbital Interactions to Control [1,2] Shifts[a]

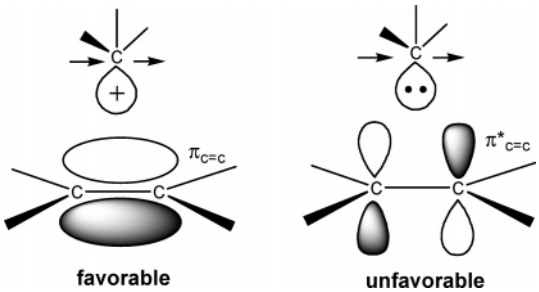

[a] The carbonium ion may slide readily on the nodeless $\pi_{C=C}$ lobe, while the carbanion undergoes the out-of-phase (symmetry forbidden) MO overlap.

rearrangements are rather rare. Scheme 2 demonstrates that carbonium ion shifts are by nature more favorable than carbanion shifts (see Figure S1 in the Supporting Information). The carbonium ion may shift on the nodeless π MO, while the carbanion must go across the nodal (symmetry forbidden) region. This is a basic problem that needs explanation: why does the carbanion benzilic rearrangement occur despite the forbiddeness?

In this work, reaction paths for the following two rearrangements were investigated computationally, and the source of the ready carbanion rearrangement was scrutinized.

$$\mathrm{Me{-}CO{-}CO{-}Me\ (biacetyl)} + \mathrm{OH^-} + (\mathrm{H_2O})_4 \rightarrow \mathrm{Me_2C(OH)COO^-} + (\mathrm{H_2O})_4$$

$$\mathrm{Ph{-}CO{-}CO{-}Ph\ (benzil)} + \mathrm{OH^-} + (\mathrm{H_2O})_4 \rightarrow \mathrm{Ph_2C(OH)COO^-} + (\mathrm{H_2O})_4$$

For the usual reaction conditions, the favored solvent with hydroxide ion is water.[1] Four water molecules are employed to solvate the hydroxide ion and to simulate the proton transfer in the third step in Scheme 1.

II. Calculation Method

The geometries of the two reacting systems, (Me−CO−CO−Me (**5**) + OH^- + $4H_2O$) and (Ph−CO−CO−Ph (**1**) + OH^- + $4H_2O$), were determined by density functional theory calculations. The B3LYP method[5] was used. B3LYP seems to be a suitable method, because it includes the electron correlation effect to some extent. The basis set is 6-31G* with diffuse orbitals[6] on the carbonyl oxygens and the hydroxide oxygen. Thus, the geometry optimizations were carried out by RB3LYP/6-31(+)G*. To assess the RB3LPY/6−31(+)G* TS geometries, RB3LYP/6-311+G(d,p) geometry optimizations were carried out for the two TS geometries and the reactant geometry of the biacetyl system. They are shown in Figure S8 (Supporting Information). A Me−CO−CO−Me + OH^- + $(H_2O)_8$ reacting system was also examined to check whether the TS geometries in Figure 1 are not affected by the additional 4 water molecules. They are shown in Figure S7 (Supporting Information). Gas-phase (without the water molecules) geometries and energies were obtained as reference data and are exhibited in Figure S5 (the Me-CO−CO−Me substrate) and Figure S6 (the Ph−CO−CO−Ph substrate), respectively.

Transition states (TSs) were characterized by vibrational analysis, which checked whether the obtained geometries have single imaginary frequencies ($\nu^{\ddagger}$s). For the biacetyl and benzil reactions, the notations TS (Me) and TS (Ph) were used, respectively. Reaction-coordinate vectors corresponding to each $\nu^{\ddagger}$ value of the biacetyl reaction are shown in Figure S2 (Supporting Information). From TSs, reaction paths were traced by the IRC (intrinsic reaction coordinate) method[7] to obtain the energy-minimum geometries. Relative energies were obtained by single-point calculations of RB3LYP/6-311+G(2d,p) SCRF=PCM[8] (solvent = water) on the RB3LYP/6-31(+)G* geometries and its zero-point vibrational energies.

All the calculations were carried out with the GAUSSIAN 98[9] program package installed on Compaq ES 40 at the Information Processing Center (Nara University of Education).

III. Computational Results and Discussions

The Biacetyl Substrate. Figure 1 shows the reaction path of the biacetyl substrate. Figure S2 (Supporting Information) shows the reactant-like complex (**5** + OH^- + $4H_2O$), where OH^- is surrounded by three water molecules in accordance with three lone-pair orbitals of OH^-. A nucleophilic water molecule, O(9)H(10)H(13), is on the C(1)−C(2) axis. When the distance of C(1)···O(9) is shortened, the OH^- addition TS (TS1(Me)) is obtained and is shown in Figure 1. The C(1)···O(9) bond formation and the bond interchange of O(9)−H(13)···O(12) → O(9)···H(13)−O(12) occur at the same time. The cooperation is shown clearly by the reaction-coordinate vectors corresponding to $\nu^{\ddagger} = 155.46i\ \mathrm{cm^{-1}}$ (Figure S2). Noteworthy is that the O(9)·····C(2) distance (2.475 Å) is slightly smaller than the O(9)·····C(1) one (2.598 Å). The one-center addition TS is as if it were a [2+1] addition. After TS1, the adduct intermediate, Me−CO^-(OH)−CO−Me (**6a**), with $4H_2O$ is generated and is shown in Figure S2. The $(H_2O)_4$ cluster is linked with the H(10)−O(9)−C(1)−O(4) moiety. The right side acetyl group may rotate around the C(1)−C(2) bond, because its length is large (=1.557 Å). After the rotation, the second adduct intermediate (**6b**) is obtained, which is slightly more stable than the first one. The second adduct (**6b**) is shown in Figure S2. In

(3) (a) von Pechmann, H. *Ber. Dtsch. Chem. Ges.* **1884**, *17*, 2534. (b) Willstätter, R.; Pfannenstiehl, A. *Justus Liebigs Ann. Chem.* **1920**, *422*, 5. (c) Wallach, O. *Justus Liebigs Ann. Chem.* **1916**, *414*, 294; **1924**, *437*, 148. (d) Schaltegger, A.; Bigler, P. *Helv. Chim. Acta* **1986**, *69*, 1666.

(4) (a) Shubin, V. G. *Top. Curr. Chem.* **1984**, *116−117*, 267. (b) Pocker, Y. In *Molecular Rearrangements*; de Mayo, P., Ed.; Wiley-Interscience: New York, 1963; p 15. (c) Collins, C. J. *Q. Rev. Chem. Soc.* **1960**, *14*, 357.

(5) (a) Becke, A. D. *J. Chem. Phys.* **1993**, *98*, 5648. (b) Lee, C.; Yang, W.; Parr, R. G. *Phys. Rev. B* **1998**, *37*, 785.

(6) Clark, T.; Chandrasekhar, J.; Spitznagel, G. W.; Schleyer, P. v. R. *J. Comput. Chem.* **1983**, *4*, 294.

(7) (a) Fukui, K. *J. Phys. Chem.* **1970**, *74*, 4161. (b) Gonzalez, C.; Schlegel, H. B. *J. Phys. Chem.* **1987**, *90*, 2154.

(8) (a) Miertus, S.; Scrocco, E.; Tomasi, J. *Chem. Phys.* **1981**, *55*, 117. (b) Miertus, S.; Tomasi, J. *Chem. Phys.* **1982**, *65*, 239.

(9) Frisch, M. J.; Trucks, G. W.; Schlegel, H. B.; Scuseria, G. E.; Robb, M. A.; Cheeseman, J. R.; Zakrzewski, V. G.; Montgomery, J. A., Jr.; Stratmann, R. E.; Burant, J. C.; Dapprich, S.; Millam, J. M.; Daniels, A. D.; Kudin, K. N.; Strain, M. C.; Farkas, O.; Tomasi, J.; Barone, V.; Cossi, M.; Cammi, R.; Mennucci, B.; Pomelli, C.; Adamo, C.; Clifford, S.; Ochterski, J.; Petersson, G. A.; Ayala, P. Y.; Cui, Q.; Morokuma, K.; Salvador, P.; Dannenberg, J. J.; Malick, D. K.; Rabuck, A. D.; Raghavachari, K.; Foresman, J. B.; Cioslowski, J.; Ortiz, J. V.; Baboul, A. G.; Stefanov, B. B.; Liu, G.; Liashenko, A.; Piskorz, P.; Komaromi, I.; Gomperts, R.; Martin, R. L.; Fox, D. J.; Keith, T.; Al-Laham, M. A.; Peng, C. Y.; Nanayakkara, A.; Challacombe, M.; Gill, P. M. W.; Johnson, B.; Chen, W.; Wong, M. W.; Andres, J. L.; Gonzalez, C.; Head-Gordon, M.; Replogle, E. S.; Pople, J. A. *Gaussian 98*, revision A.11.1; Gaussian, Inc.: Pittsburgh, PA, 2001.

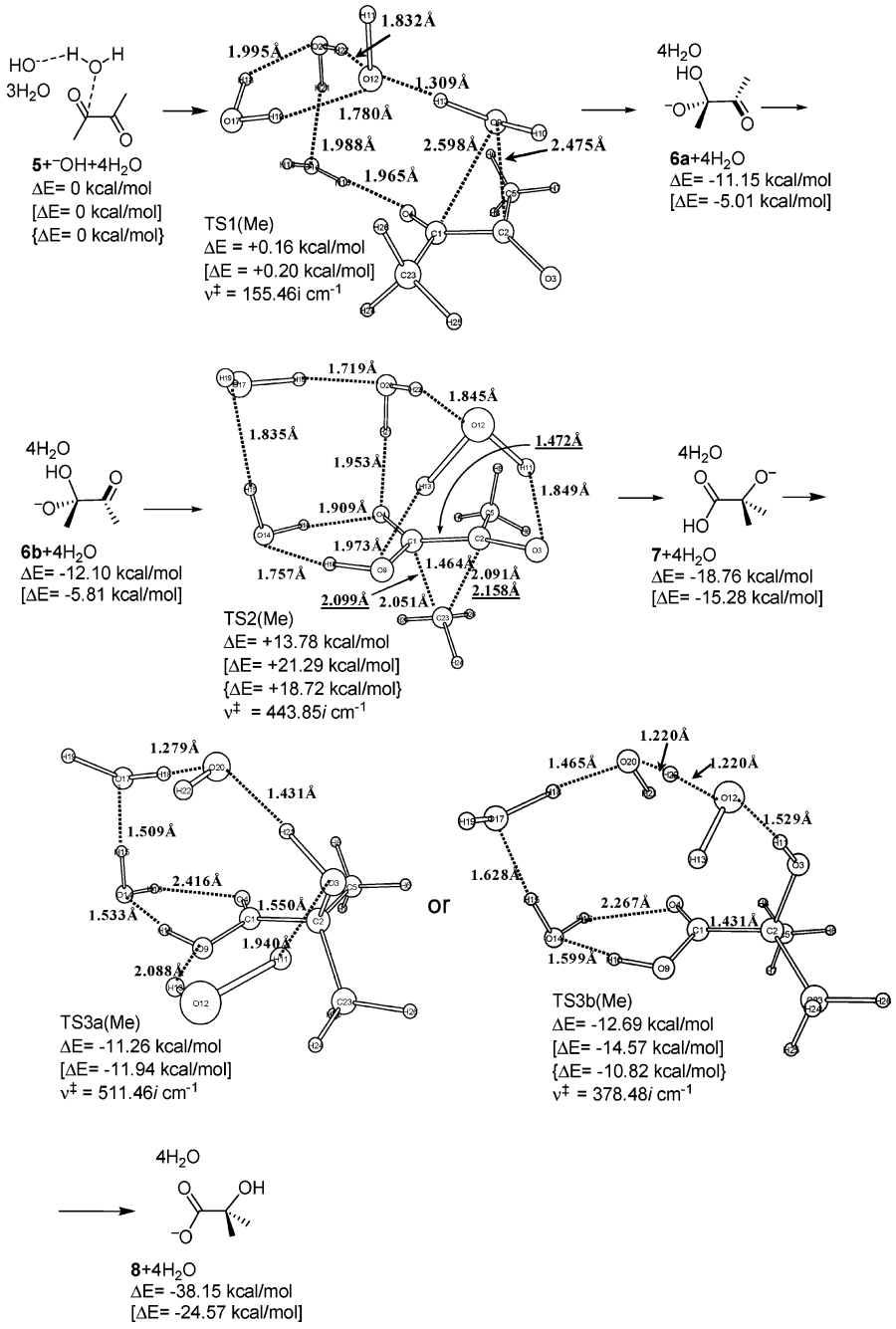

FIGURE 1. TS geometries in the reaction Me−CO−CO−Me + OH^- + $(H_2O)_4$ → MeC(OH)COO^- + $(H_2O)_4$. Δ*E* values without and with square brackets are RB3LYP/6-31(+)G* and RB3LYP/6-311+G(2d,p) SCRF=PCM relative energies, respectively. Values in braces, { }, of TS2(Me) and TS3b(Me) are those calculated by CCSD(T)/6-31(+)G*. RB3LYP/6-31(+)G* zero-point vibration energies are included in them. The underlined distances are those optimized in the gas phase (without $4H_2O$ molecules). In the gas phase, there are no precursor (**5** + OH^-) and proton-transfer TS (TS3 (Me)). Except for these, gas-phase data are in Figure S5 of the Supporting Information.

this adduct, a dihedral angle ∠C(23)−C(1)−C(2)−O(3) is −103.89°, which indicates that the methyl group, C(23)H(24)H-(25)H(26), is ready to migrate along the C(1)−C(2) bond.

The migration TS geometry was obtained (TS2(Me)) and is shown in Figure 1. The system is composed of pyruvic acid (HOOC−CO−Me), the migrating methyl anion, and $(H_2O)_4$.[10] The C(1)···C(23) and C(2)···C(23) distances are nearly 2.0 Å. This value is the typical one for formation and cleavage of the C−C bond at TS.[11] After TS2, a system composed of HOOC−$C(Me)_2O^-$ (**7**) and $(H_2O)_4$ was obtained and is exhibited in Figure S2. The alkoxide ion form C(2)−$O(3)^-$ is unstable and an isomerization via proton relay of either route a or route b is likely (Scheme 3). The two routes were investigated, and the concerted proton-relay TSs were determined. They are shown

(10) The migrating TS (TS2(Me)) might have a singlet biradical character. The character was checked in the (HOOC−CO−Me + Me)$^-$ system by the use of the broken-symmetry natural orbital occupations. If the system is ionic, the occupation is either 2 or 0 in natural orbitals. If the system is the singlet biradical, noninteger occupations (e.g., 1.5 and 0.5) are brought about. As a result of the natural-orbital calculation, the occupation was confirmed to be completely 2 or 0, and the migration is of the ionic character.

(11) Houk, K. N.; Li, Y.; Evanseck, J. D. *Angew. Chem., Int., Ed.* **1992**, *31*, 682.

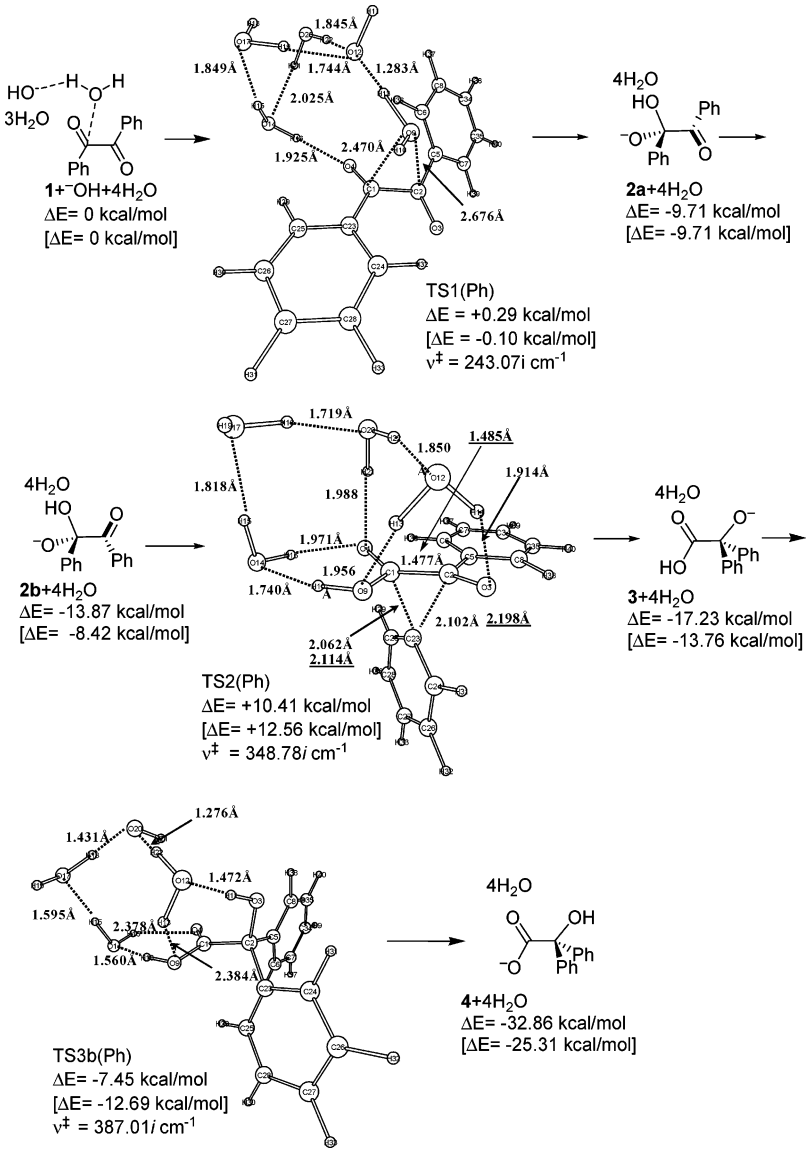

FIGURE 2. TS geometries in the reaction Ph−CO−CO−Ph + OH^- + $(H_2O)_4$ → $Ph_2C(OH)COO^-$ + $(H_2O)_4$. **1**, **2**, **3**, and **4** are defined in Scheme 1. Gas-phase data are in Figure S6 of the Supporting Information.

SCHEME 3. Two Routes (a and b) To Cause the Isomerization HOOC−CMe_2O^- (7) → $^-OOC-Me_2OH$ (8) via Proton Relays[a]

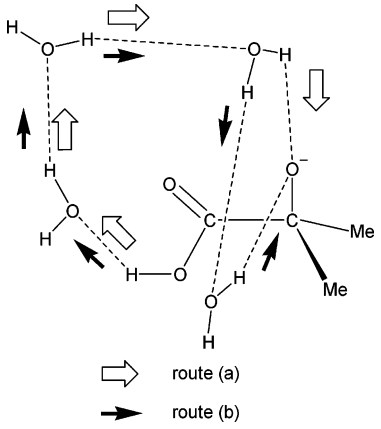

[a] Three water molecules are involved in route a, while four water molecules are in route b. The direct proton transfer (without the water molecules) was computed to be absent.

in Figure 1 as TS3a(Me) and TS3b(Me), respectively. Activation energies of the two routes are compared, and route b is found to be more favorable than route a. Thus, the employed water tetramer works fully as a reactant in the proton relay.

The relay pattern is not affected by the additional four water molecules (Figure S7-3 in the Supporting Information). The product (before acid workup), $Me_2COH-CO_2^-$ (**8**) + $(H_2O)_4$, is obtained after the proton relay, TS3b. The product geometry is shown in Figure S2 and is most stable among the species in Figure 1. Figures 1 and S2 are reviewed. The reaction is composed of the OH^- addition, the rotation isomerization of the adduct intermediate, the methyl migration, and the proton relay. The OH^- addition and removal are thought to be in equilibrium, i.e., Me−CO−CO−Me + OH^- ⇄ Me−CO(OH)−CO−Me^-, because the energetic stabilization [$\Delta E = -5.01$ kcal/mol] is almost canceled out by the entropy loss, $\Delta S° = -14.41$ cal/(mol·K), leading to $\Delta G° = -5.01 - (-14.41) \times 300/1000 = 0.69$ kcal/mol. The rate-determining step is the methyl migration with the highest ΔE. The OH^- addition and Me^- migration take place on the 1,2-diketone skeleton. Its

SCHEME 4. Charge-Transfer (CT) Interactions To Cause the Migrations

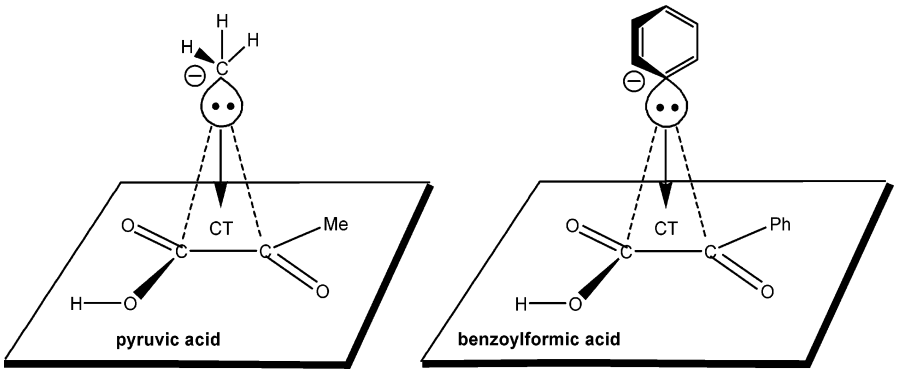

specific reactivity will be discussed in terms of the FMO theory in the next section.

The Benzil Substrate. Figures 2 and S3 (Supporting Information) show geometric changes along the second reaction, Ph-CO−CO−Ph (**1**) + OH^- + $(H_2O)_4$ → $Ph_2C(OH)COO^-$ (**4**) + $(H_2O)_4$. Figure S3 shows the precursor geometry, where the nucleophile OH^- is not in contact with the electrophilic center, C(1). In TS1(Ph) of Figure 2, the nucleophilic addition, O(9)H-(10) → C(1), and the H(13) shift occur simultaneously. As is observed in Figure 1, the [2+1]-like bridge form is involved. Two phenyl groups are distant from the hydrogen bond network and do not interfere with the OH^- addition and the proton relay. After TS1(Ph), the first one-center adduct intermediate (**2a** + $4H_2O$) is afforded (Figure S3). Its rotation isomerization leads to the second adduct, **2b** + $4H_2O$ (Figure S3). One phenyl group is ready to migrate along the C(1)−C(2) bond. The phenyl migration TS, TS2(Ph), is shown in Figure 2, where the triangle bridge form is similar to that in Figure 1. The nonmigrating phenyl group is coplanar with the reaction-center skeleton; the conjugation is expanded in the α-oxo-carboxylic acid plane. After TS2(Ph), the alkoxide intermediate (**3**) and $4H_2O$ are obtained (Figure S3). Hydrogen bonds are formed to cause ready proton relays toward the carboxylate product (**4**). The relay TS, TS3b(Ph), is exhibited in Figure 2. There, the hydrogen bond directionality is beautifully sustained via the water tetramer. After TS3b(Ph), the carboxylate **4** + $4H_2O$ is generated (Figure S3).

The phenyl groups are not obstacles (steric crowd) in the reaction of Figures S3 and 2. The reaction paths are similar to

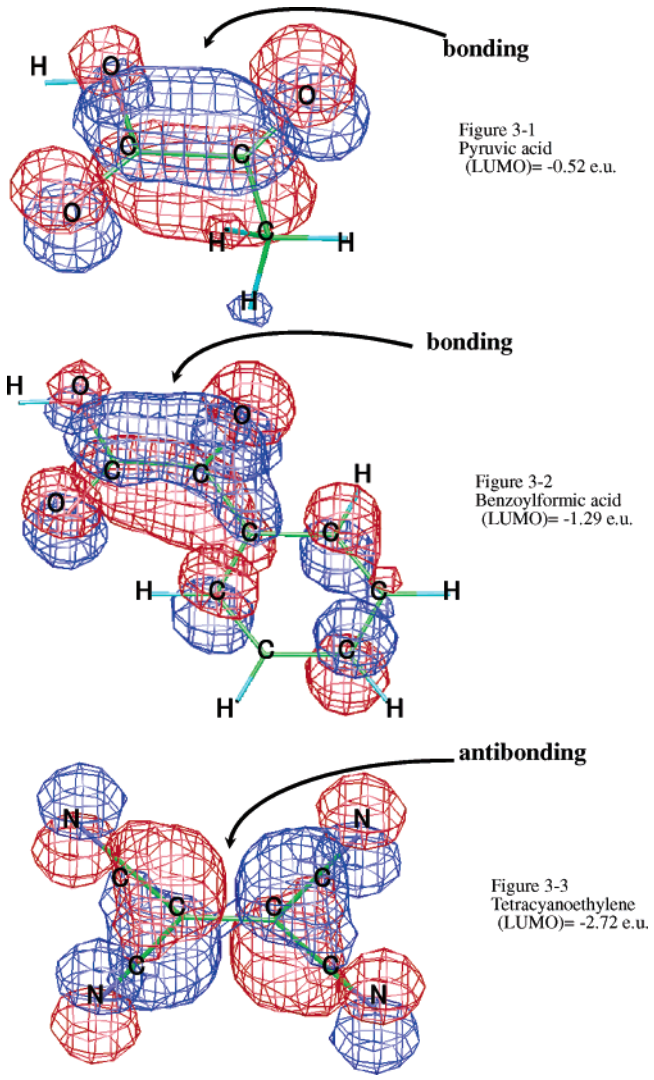

FIGURE 3. LUMOs of pyruvic acid, benzoylformic acid, and tetracyanoethylene. ϵ(LUMO) is the orbital energy of LUMO.

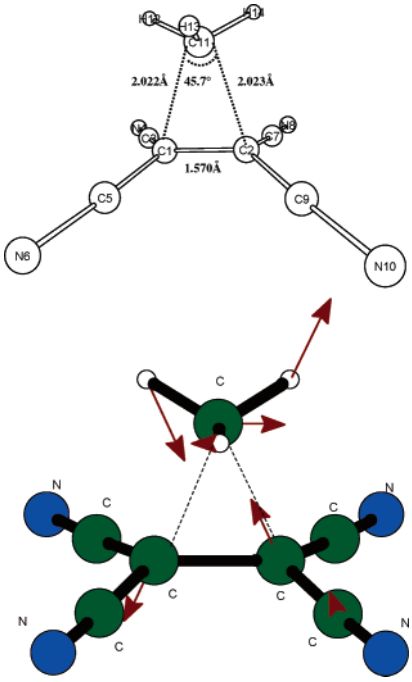

FIGURE 4. Optimized transition state structure and reaction coordinate vectors of $(Me^-)(TCNE)$ → $(TCNE)(Me^-)$.

SCHEME 5. In-phase and Out-of-Phase Combinations of Two $\pi^*_{C=O}$ Orbitals

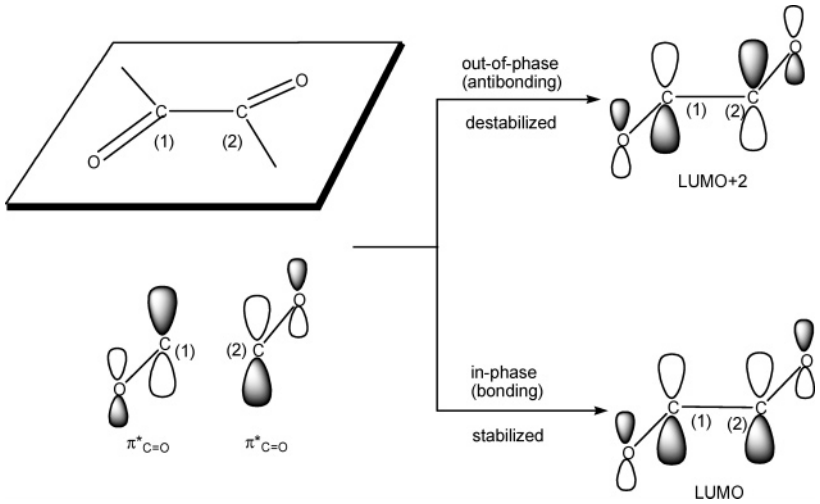

those in Figures S2 and 1. The rate-determining step is the Ph migration TS, TS2(Ph) with the highest ΔE.

IV. FMO Analyses

The Me and Ph migration steps were examined. The migrating groups were confirmed to be anionic (e.g., −0.22 for the Me group of TS2(Me) in Figure 1) by the Mulliken populations. Then, the main orbital interaction is the charge transfer (CT) from the carbanion lone-pair orbital to LUMO of either pyruvic acid or benzoylformic acid (Scheme 4). LUMOs of the two acids along with that of tetracyanoethylene (TCNE) are depicted in Figure 3. LUMOs of the two acids are the bonding (nodeless) orbitals on the two carbonyl carbon atoms. On the contrary, LUMO of TCNE is antibonding as shown in the right of Scheme 2. The two acids and generally 1,2-diketones have the common bonding property of LUMO's. LUMO is composed of the bonding (in-phase) combination of two π^*(C═O) MO's (Scheme 5). The π^*(C═O) MO has a larger lobe on the carbonyl carbon than that on the carbonyl oxygen. The in-phase combination of those vacant MO's gives a large nodeless lobe on the C(1)−C(2) region.

On the nodeless lobe, the carbanion may migrate readily. On the contrary, the carbanion may not move readily on the TCNE LUMO, which is antibonding along the C1−C2 axis. In fact, a remarkably large activation energy (+66.6 kcal/mol) was calculated in a model system, (Me^-)(TCNE) → (TCNE)(Me^-) (Figure 4).[12] The large energy for the TCNE and Me^- system demonstrates that the charge controlled[13] carbanion migration is unlikely.

In Figures 1 and 2, OH^- nucleophilic addition TSs forming O(9)−C(1) bonds have been shown. Their TS geometries are as if they were three-centered (Scheme 6). The bridged forms come from the CT interaction where a lone-pair orbital of the nucleophile is directed to the middle of LUMO (the largest spatial extension) of the 1,2-diketone substrate.

SCHEME 6. [2+1]-like Addition on the Nodeless Lobe of LUMO in Figures 1 and 2

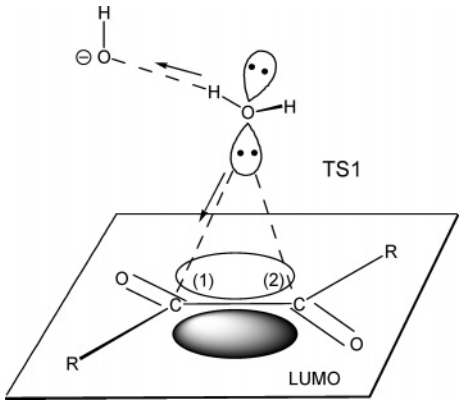

Before the migration TSs, C(1)−C(2) distances are relatively large, 1.558 (**6b**+4H_2O in Figure S2) and 1.566 Å (**2b**+4H_2O in Figure S3), respectively. They become short, 1.464 (TS2-(Me) in Figure 1) and 1.477 Å (TS2(Ph) in Figure 2) at TSs. The shortening is ascribed to the gain of the electronic charge of LUMO via the CT interaction and the consequent reflection of the LUMO bonding (in phase) character on the C(1)−C(2) axis. On the contrary, the C(1)−C(2) bond in the TCNE moiety is long (1.590 Å in Figure 4). The antibonding LUMO (Figure 3-3) of TCNE cannot accept the electronic charge from the methyl anion and accordingly the C(1)−C(2) bond remains long during the migration (Figure S4 in the Supporting Information).

V. Concluding Remarks

In this work, reaction paths of base-catalyzed rearrangements of two 1,2-diketones forming respective anions of α-hydroxy acids have been investigated. They are composed of OH^- addition, C−C rotation, carbanion [1,2] migration, and proton relay toward the product anions. The rate-determining step has been confirmed to be the carbanion migration with the calculated highest ΔE.

The cabanion [1,2] migration is basically unlikely (forbidden) as is shown in the right of Scheme 2. However, the 1,2-diketones

(12) The following small CT interaction contributes slightly to the carbanion shift. The antisymmetric CT interaction is substantiated by the shape of HOMO of TS shown in Figure S4(b) (Supporting Information).

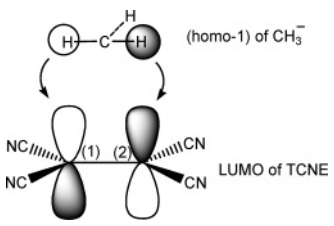

(13) Klopman, G. K. *J. Am. Chem. Soc.* **1968**, *90*, 223.

have nodeless and large lobes of LUMOs which make the migration ready. The C(1)−C(2) bond of the α-diketone works not as the electrophilic (cationic) site but as the moiety of the 4π electron system. In fact, the methyl anion migration is unlikely on the 2π electron system, TCNE. Thus, carbocation and carbanion rearrangements are summarized in terms of the Woodward−Hoffmann[14] and Hückel rules. The carbocation migration occurs in a two electron reacting system (zero from the cation and two from the olefin), which is a favorable case in the $(4n+2)$ rule, $n = 0$. The system of the carbanion shift on the olefin has 2+2 electrons, where the former two belong to the carbanion lone-pair orbital. This case is symmetry forbidden and is of the anti-Hückel rule (unfavorable). The system composed of the carbanion and 1,2-diketone has 2+4 electrons, which is fit for the symmetry allowed and ready migration.

(14) Woodward, R. B.; Hoffmann, R. *The Conservation of Orbital Symmetry*; Verlag Chemie: New York, 1970; Chapter 3.1.

Supporting Information Available: Figures S1−S8 and the Cartesian coordinates of the optimized geometries of Figures 1, 2, S2, and S3. This material is available free of charge via the Internet at http://pubs.acs.org.

JO051862R